Int J Environ Res (2022) 16:20
https://doi.org/10.1007/s41742-022-00399-5

RESEARCH PAPER

# Optimization of Silica Extraction from Rice Husk Using Response Surface Methodology and Adsorption of Safranin Dye

Melis Gun[1] · Hudaverdi Arslan[1] · Mohammed Saleh[2] · Mutlu Yalvac[1] · Nadir Dizge[1]

Received: 24 September 2021 / Revised: 15 February 2022 / Accepted: 4 March 2022


## Abstract

This study aims to extract and optimize silica from rice husk (RH) using the response surface methodology. The effects of temperature, potassium hydroxide to rice husk ratio (KOH: RH), and exposure time were modeled. The developed model was significant and adequately precise to navigate the design space with a percentage of 93.19%. Based on the *F* value for the model terms, the KOH: RH ratio is the most important factor, followed by time, then temperature. Based on XRF analysis, the maximum yield was 55%. The extracted silica was utilized for Safranin dye adsorption from aqueous solutions. The affecting factors like; pH, adsorbent amount, initial concentration, and time were optimized; to achieve maximum adsorption efficiency. The optimum conditions for Safranin adsorption occurred at pH 8, adsorbent dose of 1 g/L, initial concentration of 25 mg/L, and contact time of 60 min. The adsorption of Safranin onto the extracted was found to be described by Langmuir isotherm.

## Article Highlights

- **Silica was extracted and optimized from rice husk (RH) using the response surface methodology.**
- **The effects of temperature, potassium hydroxide to rice husk ratio (KOH: RH), and exposure time were modeled.**
- **Based on XRF analysis, the maximum silica extraction yield was 55%.**
- **The optimum conditions for Safranin adsorption were also investigated.**

**Keywords** Silica extraction · Response surface methodology · Safranin adsorption

## Introduction

Rice is an important agricultural product and it is included in all nutritional lists worldwide (Wang et al. 2017; Rodríguez-Restrepo et al. 2020). According to FAO 2021 data, 162,191,000 decares of rice were cultivated and 744,356,000 tons of products were obtained globally in the last 2 years (Barker et al. 2000).

Rice husk is an agricultural waste generated in large quantities after rice production (Thamnarathip et al. 2016; Khan 2015; Jaya 2020). About 20–33% by weight of paddy is rice husk (Quispe et al. 2017; Shafie et al. 2012). Rice husk contains 28–30% inorganic and 70–72% organic compounds (Korotkova et al. 2016). The organic part consists of cellulose, hemicellulose, and lignin. Depending on the characteristics of the paddy production area, cellulose, hemicellulose, and lignin can vary between 28.6–41.5%, 14.0–28.6%, and 20.4–33.7%, respectively (Muhammad et al. 2013; Lim et al. 2012). The most critical component of the inorganic part is silica ($SiO_2$). $SiO_2$ forms the skeleton of the husk. The silica in the raw husk is reported as 15–20% by weight (Pang et al. 2021). However, $SiO_2$ in rice husk ash can be found in amounts ranging from 60 to 70% (Nuamah et al. 2012) to 90–98% (Phonphuak and Chindaprasirt 2015; Feng et al. 2018), it is possible to list other components in rice husk ash as $K_2O$, MgO, CaO, $P_2O_5$, and small amounts of Na, Fe, and Al (Korotkova et al. 2016; Moraes et al. 2014; Van et al. 2014). The calorific value of rice husk is between 13.4 and 17.4 MJ/kg, depending on the type of rice and the region where it is grown (Della et al. 2006; Wang et al. 2012;

✉ Nadir Dizge
ndizge@mersin.edu.tr

1 Department of Environmental Engineering, Engineering Faculty, Mersin University, Mersin, Turkey

2 National Agricultural Research Center (NARC), Jenin, Palestine

Published online: 22 March 2022

Alvarez et al. 2014). Due to the valuable components, many researchers have investigated the beneficial use of rice husk.

The structure and properties of raw rice husk also depend on the rice husk (RH) combustion temperature. RH is obtained under various combustion temperatures (400–900 °C). The specific surface area and pore volume of RH decreased with increasing combustion temperature when solid combustible materials were mostly burned. The density of the amorphous silica structure of RH decreases with increasing temperature while the Si–O–Si bond angle increases with temperature. Choudhary et al. (2021) obtained $Na_2SiO_3$ solution by mixing the rice husk ash and they obtained by burning the rice husk after to be cleaned from impurities at 700 °C for 6 h with 1 N NaOH (Eq. 1). By adding 1 N HCl to the solution, they provided the precipitation of silica particles at pH 7 (Eq. 2) (Choudhary et al. 2021).

$$SiO_2 + 2NaOH \rightarrow {}^1\!/_4 Na_2SiO_3 + H_2O \quad (1)$$

$$Na_2SiO_3 + 2HCl \rightarrow SiO_2 + H_2O + 2NaCl. \quad (2)$$

So far, silica nanoparticles have been obtained from different sources and used for different applications. For example, amorphous silica was obtained by burning rice husk at approximately 700 °C and used in mortar production instead of Portland cement as an environmentally friendly mortar (Marangon et al. 2021). In another study, hydrophobic wrinkled silica nanoparticles (WSNs) were obtained by surface functionalization with perfluorodecyltriethoxysilane (PDTES) by chemical vapour deposition (CVD) (Pota et al. 2021). The lipase was immobilized to the hydrophobically functionalized surface. The biocatalyst was tested in the hydrolysis and transesterification of sunflower seed oil and compared to free lipase. The reaction yields of 87% for immobilized lipase and 75% for free lipase were obtained for hydrolysis. However, the reaction yields of 93% for immobilized lipase and 56% for free lipase were obtained for transesterification (Pota et al. 2021). Rice husk ash was used for inorganic fertilizers and it increased the pH in acid soils (Saranya et al. 2018). It was reported that substitution of rice husk ash @ 10 t $ha^{-1}$ along with 50% of recommended K could enhance maize growth and growth parameters. Silica obtained from RHA was used for biodiesel production (Chen et al. 2013). Rice husk ash was modified with $Li_2CO_3$ to obtain $Li_2SiO_3$. The transesterification of soybean oil with methanol was carried out in the presence of the catalyst at atmospheric pressure. 99.5% conversion to biodiesel was achieved under the optimal reaction conditions of a methanol/oil molar ratio of 24:1, a 4% catalyst amount, and a reaction temperature of 65 °C for 3 h (Chen et al. 2013).

The use of synthetic dyestuff in wide ranges of applications increases day by day (Bilici et al. 2022). Accordingly, 10–15% of the used dyes enter the environment as wastes, which cause harm to the human being and the surrounding environment (Gupta and Suhas 2009). The presence of dyestuff in the water bodies obstacles light penetration into the aquatic life and produces several types of harmful chemicals, which negatively affect the flora, fauna, and human beings (Arslantaş et al. 2022). Safranin dye, which is a cationic dye, is a common dye utilized as a colorant for textile, tannin, cotton, fibers, wool, silk, leather, and paper (Shah 1998). Despite its wide applications, safranin had dangerous impacts on the human body. Eye irritation, cornea and conjunctiva injuries, and skin and respiratory tract irritation are examples of the safranin detrimental influences (Gupta et al. 2007). Thus, the removal of safranin from the solutions has the researcher's interest. Many treatment methods were employed in dye removal. Over those methods, the adsorption approach was extensively utilized since the adsorption achieves high removal efficiency with minimal costs and fewer requirements (Mohamed et al. 2020; Kamal 2020). Several adsorbents types were used in safranin removal. In this context, Preethi et al. (2006) removed safranin from the aqueous solution by corncob-activated carbon (Preethi et al. 2006). Fayazi and colleagues (2015) utilized magnetic mesoporous clay in safranin removal (Fayazi et al. 2015). Lignin nanoparticle-g-polyacrylic acid adsorbent was also used for the same objective (Azimvand et al. 2018).

In this study, silica was extracted from rice husk (RH). The response surface method (RSM) was employed to control the extraction method based on temperature, potassium hydroxide to rice husk ratio, and exposure time factors. RSM is an optimization tool that can handle different parameters at the same moment (Saleh et al. 2021a). RSM is based on a group of mathematical algorithms, and statistical techniques that an also determine the interaction between the parameters. In this way, RSM requires fewer experiment sets, which reflects positively on the time and cost related to the optimization process (Saleh et al. 2021b). Box-Behnken design was used for silica extraction optimization since the method uses face points, which is more practical than other methods (Box et al. 2005). Silica-based rice husk was used for safranin dye adsorption from the aqueous solutions. The use of silica from waste sources is thought to be a green solution for safranin removal. The affecting parameters (pH, adsorbent amount, initial concentration, and time) were optimized to achieve maximum adsorption efficiency.

## Material and Method

### Preparation and Characterization of the Adsorbent

Rice husk was obtained from a pulses company located in Mersin. Rice husk was dried in the oven (Hareus) at

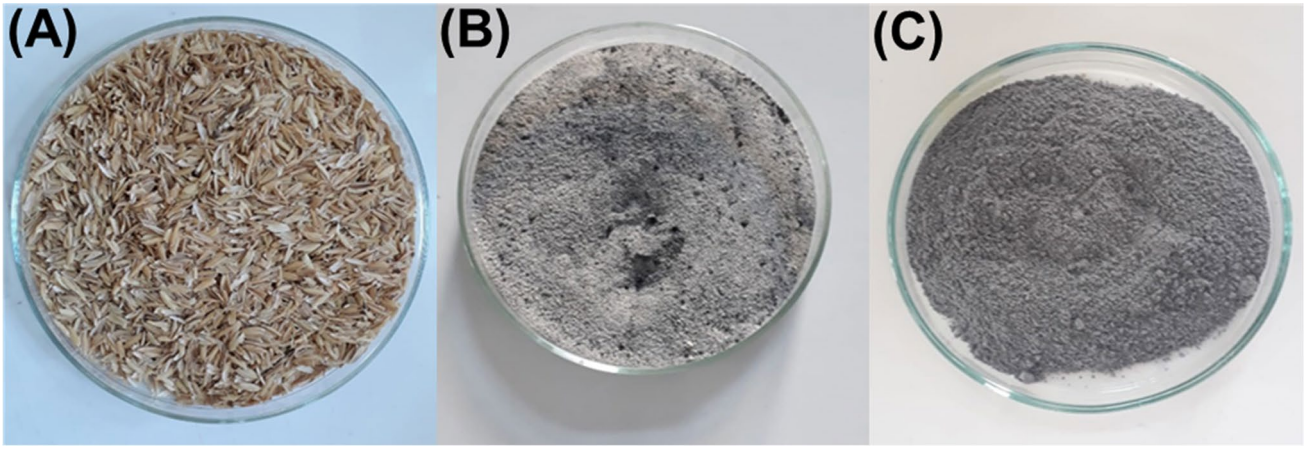


**Fig. 1** **A** Untreated rice husk, **B** carbonized rice husk at 350 °C, **C** rice husk ash mixed with KOH and burned in a muffle furnace

**Table 1** Variables ranges for the RSM

| Variable | Unit | Factor | Low | High |
|---|---|---|---|---|
| Temperature | °C | A | 700 | 900 |
| KOH:RH | – | B | 0.5 | 2 |
| Time | Min | C | 60 | 180 |

105 °C and it was ground with a ring mill and passed through a 35 mesh sieve. The prepared raw rice husk was carbonized at 350 °C for 2 h and the rice husk ashes (RHA) were obtained. These ashes were mixed with potassium hydroxide (KOH) and burned in the muffle furnace (Protherm) (Fig. 1).

Response surface method (RSM) was employed to optimize the silica extraction process from the rice husk. The extracted silica ratio was assessed based on temperature, potassium hydroxide to rice husk ratio, and exposure time. Table 1 shows the ranges of the variables.

The variables ranges were identified using the preliminary experiments. To model the effect of these variables on the amount of the extracted silica, 17 experiments were fulfilled. The results were analyzed with the help of Design Expert V11 software.

The energy-dispersive X-ray spectroscopy (EDX) was employed to quantify the composition of the elements at the adsorbent surface. X-ray fluorescence (XRF- Panalytical Zetium) was utilized for the chemical composition determination. The surface area, the total pore volume, and the pore diameter were characterized using Brunauer

**Table 2** Safranin properties (Vasanth Kumar and Sivanesan 2007)

| | |
|---|---|
| Chemical formula | $C_{20}H_{19}ClN_4$ |
| Chemical structure | 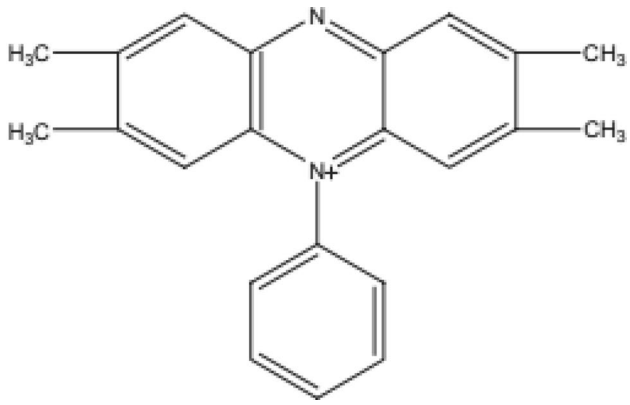 |
| Wavelength | 517–530 |
| Color | Red |
| Ionization | Basic |
| Molecular weight | 350.8 |

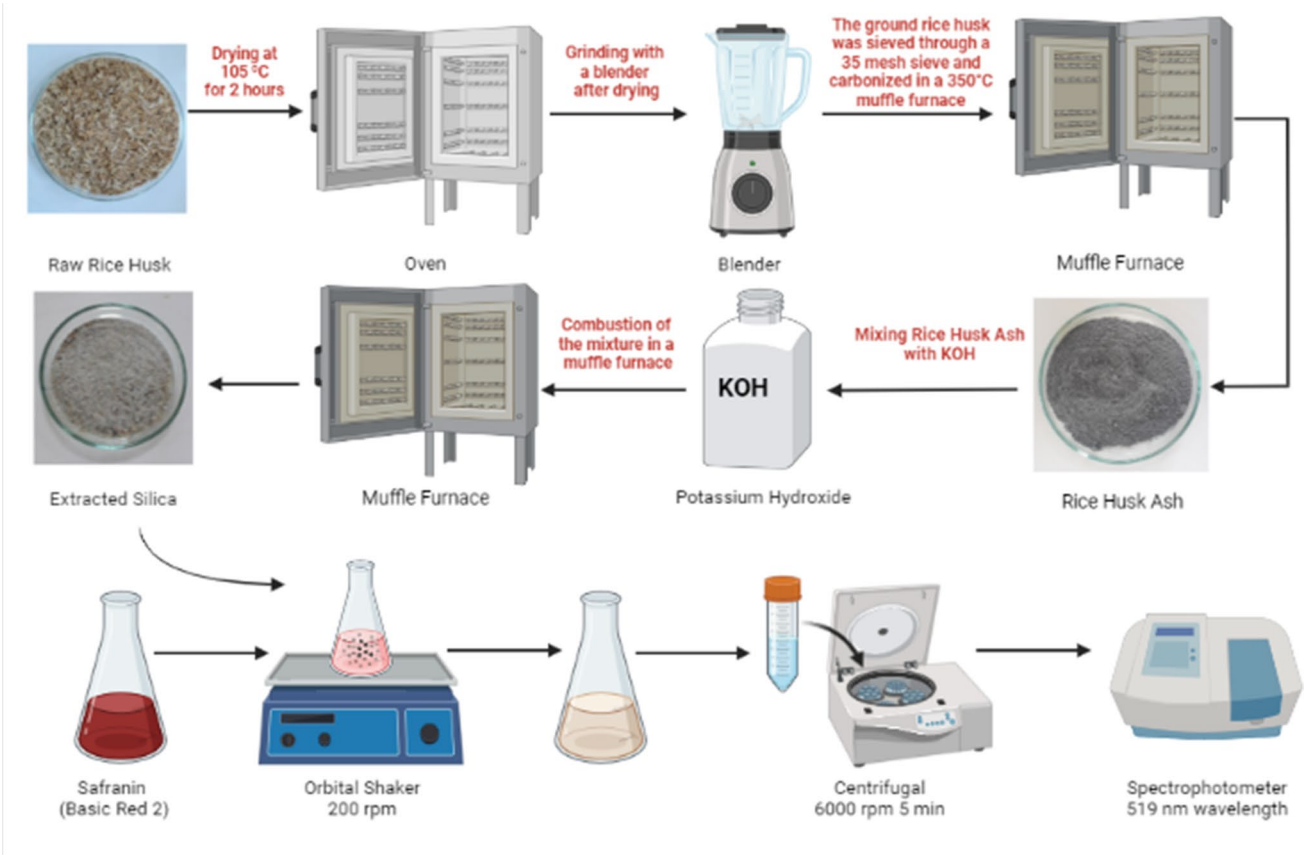


**Fig. 2** A schematic scheme of adsorbent preparation and dye adsorption

Emmett-Teller (BET) analysis via MicroActive for TriStar II Plus 2.00. The functional groups at the surface of the RHA adsorbent were identified using Fourier transform infrared spectroscopy (FT/IR-6700, Jasco) for the bands 450-4000 $cm^{-1}$.

## Dye Preparation

Safranin (Basic Red 2) is a catatonic synthetic dye with a chemical formula $C_{20}H_{19}ClN_4$ and a molecular weight of 350.8 g/mol. A stock solution with 1000 ppm was prepared. In the experiments, 0.1 M sodium hydroxide (NaOH) and 0.1 M hydrochloric acid (HCl) were used to adjust pH to desired values. Table 2 shows the dye properties.

A schematic scheme is shown in Fig. 2 to show the idea of this work.

## Adsorption Experiments

In the experiments; pH, adsorbent amount, initial dye concentration, and time were optimized as parameters. 100-mL solution volume was used in all experiments. As a result of the experiment, the removal efficiency (%) and the adsorption capacity ($q_e$) (mg/g) were calculated using Eqs. 3 and 4, respectively (Castillo et al. 2018).

$$\text{Efficiency\%} = (C_i - C_e)/C_i \times 100\% \quad (3)$$

$$q_e = (C_i - C_e) \times V/m \quad (4)$$

where $C_i$ and $C_e$ are the initial concentration and final concentration (mg/L); $q_e$ is the solid phase concentration (mg/g); $V$ is volume of the solution in (L); and $m$ is the extracted mass (g).

## Adsorption Isotherms

Langmuir and Freundlich's isotherms were used to examine the relationship between adsorbent and adsorbed substances. The Langmuir isotherm is based on the assumption of single-layer adsorption occurring on the homogeneous surface of the adsorbent (Eq. 5) (Langmuir 1918). Freundlich isotherm expresses an empirical equation in the adsorption process (Eq. 6) (Freundlich 1906).

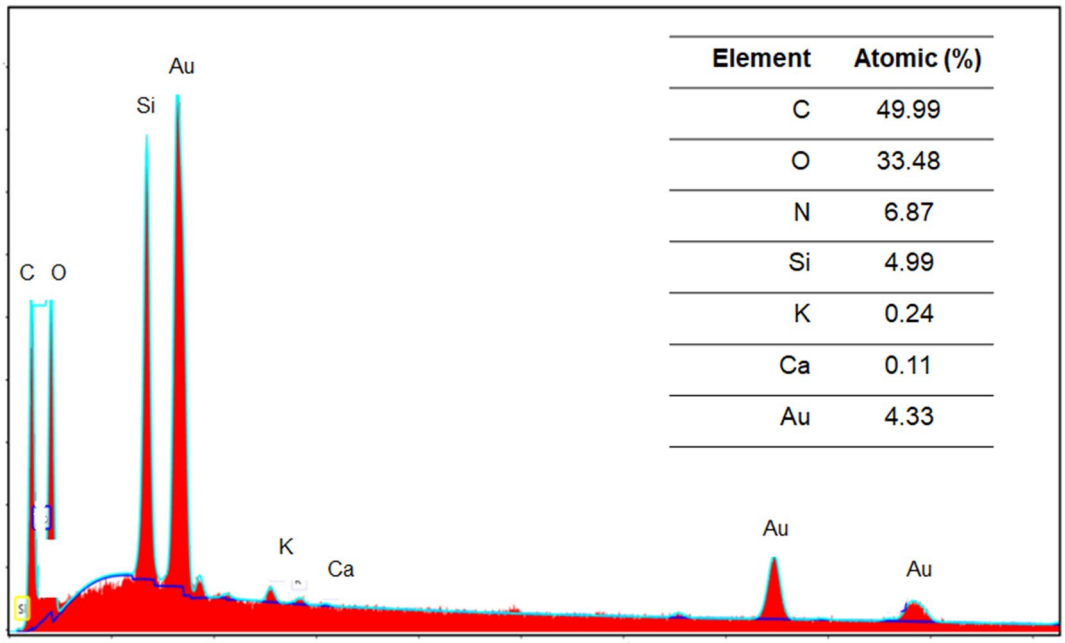


| Element | Atomic (%) |
|---|---|
| C | 49.99 |
| O | 33.48 |
| N | 6.87 |
| Si | 4.99 |
| K | 0.24 |
| Ca | 0.11 |
| Au | 4.33 |

**Fig. 3** EDX pattern of raw rice husk

$$q_e = \frac{q_m K_L C_e}{1 + K_L C_e} \tag{5}$$

$$q_e = K_A C_e^{1/n} \tag{6}$$

where, $q_e$ and $C_e$ are the adsorption capacity (mg/g) and the concentration (mg/L) at the equilibrium. $K_L$, and $K_A$ are Langmuir and Freundlich constants, respectively. $q_m$ is the maximum adsorption capacity (mg/g). $1/n$ is the heterogeneity factor.

## Results and Discussions

### Characterization of the Rise Husk

EDX analysis was performed for raw rice husk as shown in Fig. 3. It was seen that the sample composed of carbon, oxygen, nitrogen, and silica. However, traces of potassium and calcium elements were found in the structure of the raw rice husk.

The structural morphology of raw rice husk, carbonized rusk husk, and rice husk ash were also investigated by SEM analysis (Fig. 4). Differences in surface morphology were observed after carbonization and calcination process. The structure of the raw rice husk had a heterogeneous structure containing small particles on it (Fig. 4A). After the carbonization of the rice husk at 350 °C, the structure changed to wavy configuration on flat ground (Fig. 4B). In addition, the number of small particles on the surface increased. After the calcination process at 900 °C, small particles disappeared and a flatter but cracked structure was obtained (Fig. 4C). It was thought that these cracks increased the adsorption efficiency.

Table 3 shows the results for the BET surface area, total pore volume, and average pore diameter for raw rice husk, carbonized rice husk, and rice husk ash. Based on Table 1, carbonized rice husk has an area of 98.66 $m^2/g$, followed by the rice husk ash and raw rice husk. The pores size determines the adsorptive properties of rice husk. The pore diameter reached 50.67 nm at a sintering temperature of 900 °C. The average pore diameter of the rice husk ash decreased compared to raw rice husk; however, it increased compared to carbonized rice husk.

FTIR was used to identify some characteristic functional groups of the rice husk. As can be seen in the Table 4, IR spectra of rice husk in the region 1200–1000 $cm^{-1}$ were considered to result from superposition of vibrations of the C–OH bond and Si–O bond in the siloxane (Si–O–Si) groups. The absorbance peak at 450 $cm^{-1}$ was due to the bending vibration of siloxane bonds. Hydroxyl groups (O–H) are usually in the range of 3200–3650 $cm^{-1}$ for alcohols and phenols, aliphatic groups (C–H) located at around 2919 $cm^{-1}$. The band appearing at 1633 $cm^{-1}$ was attributed to the carbonyl (C=O) groups (Morcali et al. 2013).

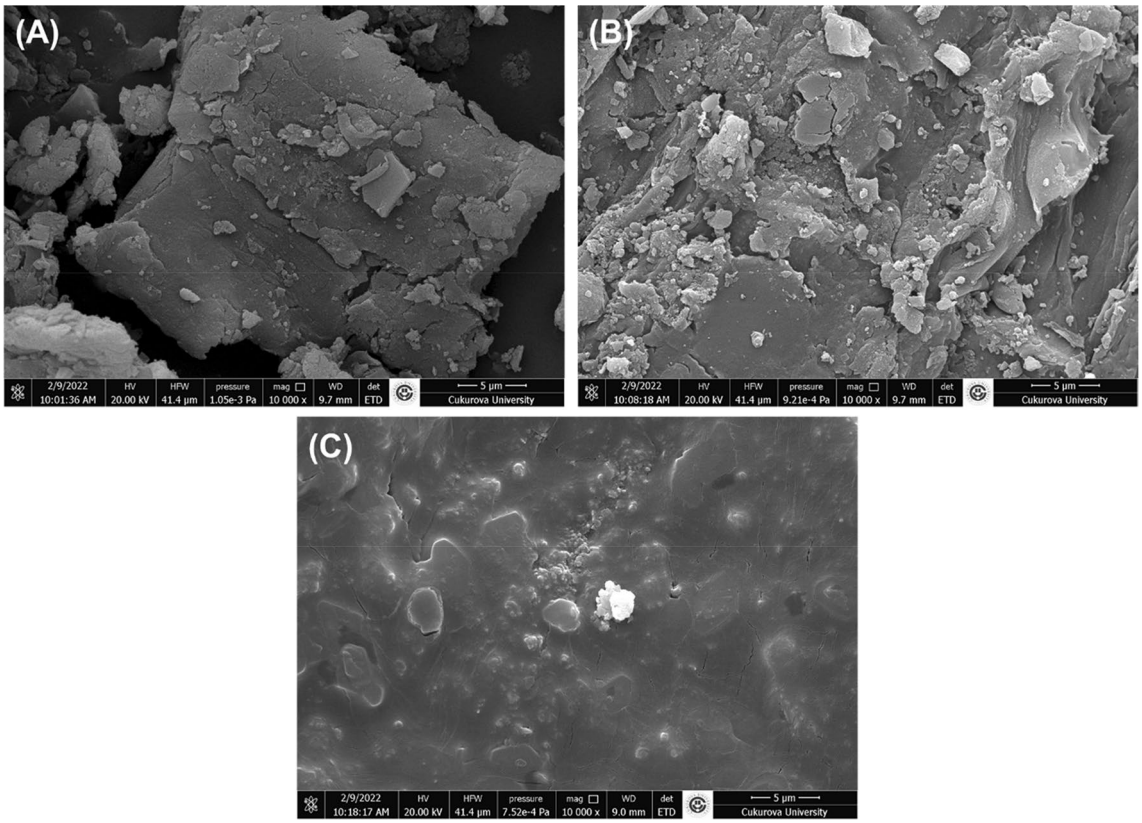


**Fig. 4** SEM images of **A** raw rice husk, **B** carbonized rusk husk, and **C** rice husk ash

**Table 3** BET analysis results of raw rice husk, carbonized rice husk, and rice husk ash

| Parameter | Unit | Raw rice husk | Carbonized rice husk | Rice husk ash |
|---|---|---|---|---|
| BET surface area | ($m^2$/g) | 0.6508 | 98.6609 | 3.4709 |
| Total pore volume | ($cm^3$/g) | 0.00172 | 0.09844 | 0.00333 |
| Pore diameter | nm | 73.02 | 11.28 | 50.67 |

**Table 4** FTIR spectra of raw rice husk, carbonized rice husk, and rice husk ash

| FT-IR peaks ($cm^{-1}$) | | | Vibrational mode |
|---|---|---|---|
| Raw rice husk | Carbonized rice husk | Rice husk ash | |
| 3337.21 | – | 3123.15 | ν(O–H) |
| 2918.73 | – | – | Symmetric ν($CH_2$) of chain |
| 1633.41 | – | 1644.98 | ν(C = O) |
| 1509.99 | – | 1361.50 | δ(C–H) |
| 1033.66 | 1047.16 | 988.34 | Si–O–Si stretching vibration |
| 790.67 | 794.53 | 876.49 | Si–C stretching vibration |
| 454.15 | 450.30 | 450.30 | Si–O–Si bending vibration |

## RSM Results for Silica Extraction from RHA

The silica extraction process from rice husk (RH) occurred in the assistant of RSM. The affecting factors on the silica extraction were modeled by the Box-Behnken method with Design Expert V11 software aiding. The samples were analyzed by the XRF analysis; to determine the silica percentages.

The XRF analysis results were fitted to 2FI, Linear, Quadratic and Cubic models to obtain the best representative model. Table 5 shows the Sequential model sum of squares for the different models.

Based on the $F$ value and $p$ value, the extracted silica is best represented by quadratic vs. 2FI models, while cubic vs. quadratic is aliased. Based on the regression coefficient ($R^2$), the quadratic model was selected. Table 6 shows model summary statistics.

**Table 5** Sequential model sum of squares

| Source | Sum of squares | Mean | *F* value | *p* value | Note |
|---|---|---|---|---|---|
| Mean vs total | 445.6129 | 445.6129 | | | |
| Linear vs mean | 16.47381 | 5.491268 | 8.008999 | 0.002812 | |
| 2FI vs linear | 4.960721 | 1.653574 | 4.183546 | 0.036815 | |
| Quadratic vs 2FI | 3.667409 | 1.22247 | 30.00918 | 0.000228 | Suggested |
| Cubic vs quadratic | 0.285156 | 0.095052 | | | Aliased |
| Residual | 0 | 0 | | | |
| Total | 471 | 27.70588 | | | |

**Table 6** Model summary statistics

| Source | Std | $R^2$ | Adjusted $R^2$ | Predicted $R^2$ | Note |
|---|---|---|---|---|---|
| Linear | 0.828032 | 0.648905 | 0.567883 | 0.300088 | |
| 2FI | 0.628694 | 0.844308 | 0.750893 | 0.345671 | |
| Quadratic | 0.201833 | 0.988768 | 0.974326 | 0.820283 | Suggested |
| Cubic | 0 | 1 | 1 | | Aliased |

**Table 7** ANOVA test for the developed model

| Source | Sum of squares | Mean | *F* value | *p* value |
|---|---|---|---|---|
| Model | 24.97474 | 4.162456 | 100.9437 | 2.31E−08 |
| A-Temperature | 1.810664 | 1.810664 | 43.91039 | 5.88E−05 |
| B-KOH:RH | 12.0285 | 12.0285 | 291.703 | 9.98E−09 |
| C-Time | 2.634642 | 2.634642 | 63.89266 | 1.19E−05 |
| AB | 3.349734 | 3.349734 | 81.23437 | 4.08E−06 |
| AC | 1.493394 | 1.493394 | 36.21629 | 0.000129 |
| $B^2$ | 3.657802 | 3.657802 | 88.70531 | 2.75E−06 |
| Residual | 0.412354 | 0.041235 | | |
| Lack of Fit | 0.412354 | 0.068726 | | |
| Pure Error | 0 | 0 | | |
| Cor Total | 25.38709 | | | |

The analysis of variance (ANOVA) test examined the model significance. The quadratic model was reduced to improve the model (Table 7).

Based on the results presented in Table 7, the F value and P value for the developed model were 100.94 and $2.31 \times 10^{-8}$, respectively, which implies the model is statistically significant. The model terms that have a *p* value less

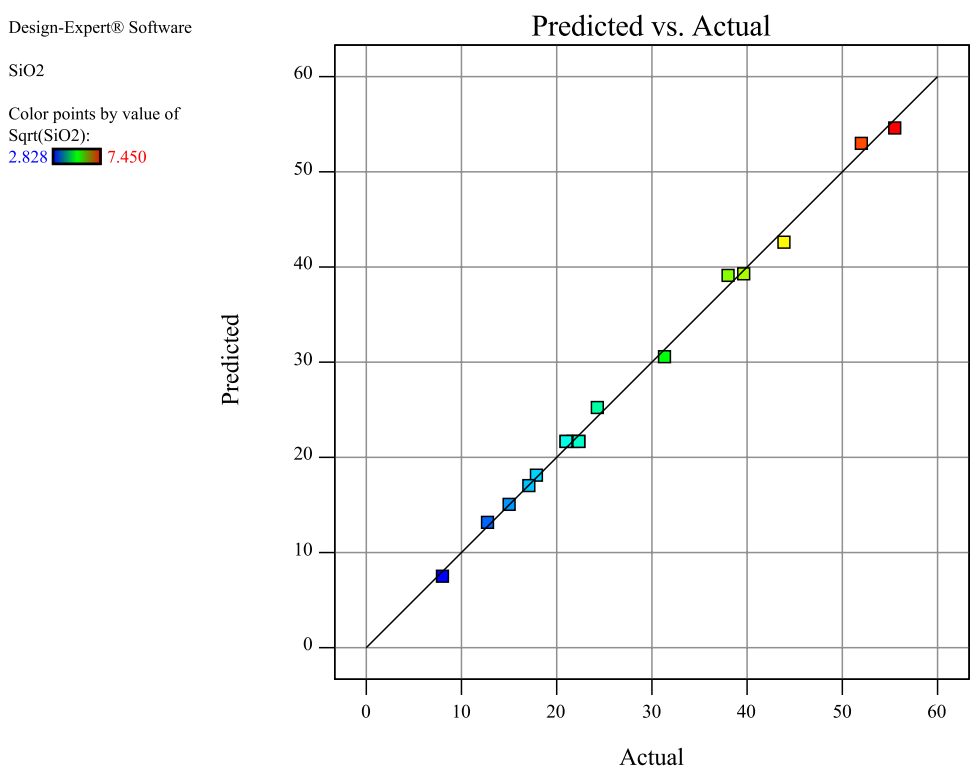


**Fig. 5** Predicted vs actual values for the silica extraction model

than 0.0500 are significant. In this case, A, B, C, AB, AC, $B^2$ are significant model terms. Based on the $F$ value for the model terms, the KOH: RH ratio is the most important factor, followed by time, then temperature. The adjusted $R^2$ and the predicted $R^2$ for the modified quadratic model were 0.9740 and 0.9319, respectively. The model was also adequately precise (33.8985 > 4), and the model can be used to navigate the design space with a percentage of 93.19%. This shows an excellent correlation between the predicted results and the actual results. Similar results were discussed previously (Saleh et al. 2019a; Deb et al. 2019). Figure 5 shows the correlation between the predicted and actual values for the silica extraction.

The actual factors equation for the extracted silica model is shown in Eq. 7.

$$\begin{aligned}\sqrt{\text{Silica}}\% = &-10.01206 + 0.022715 \times \text{Temperature} + 3.99594 \\ &\times \text{KOH}:\text{RH} + 0.091034 \times \text{Time} - 0.012202 \times \text{Temperature} \\ &\times \text{KOH}:\text{RH} - 0.000102 \times \text{Temperature} \times \text{Time} + 1.65214 \times (\text{KOH}:\text{RH})^2\end{aligned} \tag{7}$$

The effects of the individual parameters on the silica extraction process were examined. Figure 6A, B show the

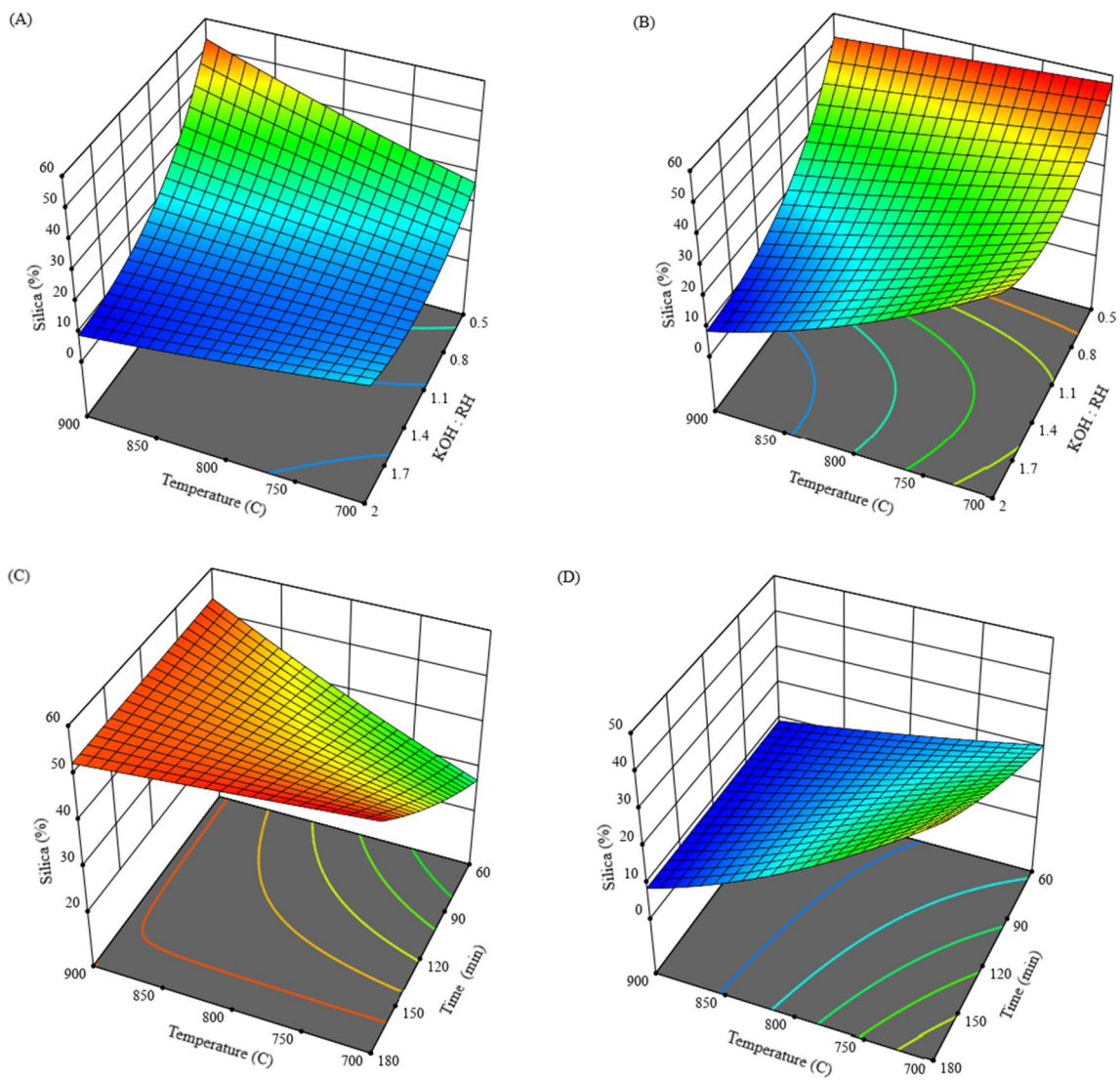


**Fig. 6** **A** The effects of temperature and the KOH: RH ratio on silica extraction at a time of 60 min. **B** The effects of temperature and the KOH: RH ratio on silica extraction at a time of 180 min. **C** The effects of time and temperature on silica extraction at a KOH: RH ratio of 0.5. **D** The effects of time and temperature on silica extraction at a KOH: RH ratio of 2

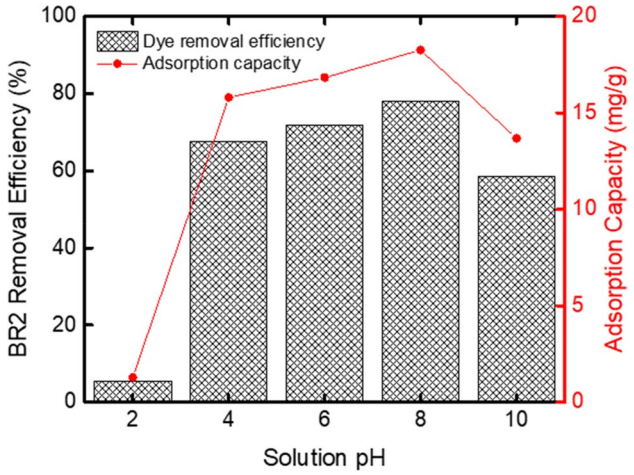


**Fig. 7** The changes in the removal efficiency and the adsorption capacity with the change in pH

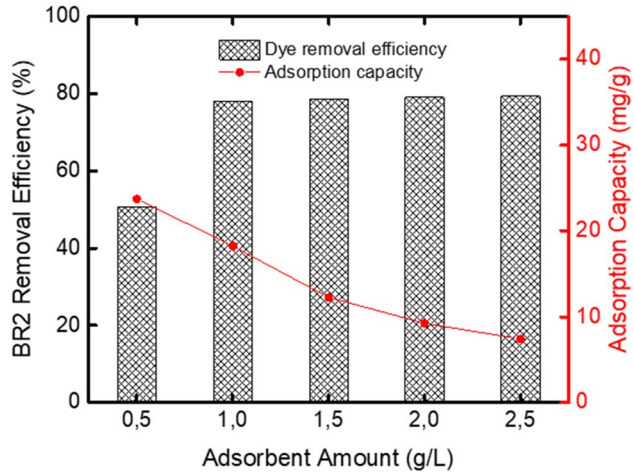


**Fig. 8** The changes in the removal efficiency and the adsorption capacity with the change in the adsorbent amount

effects of temperature and the KOH: RH ratio on silica extraction. For an exposure time of 60 min, the extracted silica increased with the increases in the temperature at low KOH: RH ratios. At 900 °C and KOH: RH ratio of 0.5, the obtained silica was 55%. With the increases in the KOH: RH ratios, the silica amount decreased with temperature increases. For a long time exposure (180 min), the amount of obtained silica had an inverse relation with the temperature for all KOH: RH ratios. Also, the silica amount decreased with the increases in the KOH: RH ratio from 57 at 0.5–35 at 2. The decreases in the silica amount had a sharper shape for the high-temperature degrees. The effects of time and temperature on the silica are presented in Fig. 6C and D. For the temperature range 700–800 °C, the amount of extracted silica increased with the increases in the exposure time. Beyond that range, the increases in time had an inverse relationship (Fig. 6C). At higher KOH: RH ratios, the increases in time had minimal effects on the silica extraction, as shown in Fig. 6D.

## Adsorption of Safranin Dye onto the Extracted Silica

### The Effect of pH

The protonation and deprotonation processes on the extracted silica surface are controlled by pH (Isik et al. 2021). In this step, 1 g/L of the extracted silica was added to 25 mg/L of the dye concentration. The mixture was agitated at 200 rpm for 60 min at room temperature (25 ± 2 °C). The changes in the removal efficiencies and the adsorption capacities with pH are shown in Fig. 7. The removal efficiency increased with the increases in pH. At pH 2, the removal efficiency and the adsorption capacity were 5.5% and 1.3 mg/g. The removal efficiency and the adsorption capacity increased sharply at pH 4 to reach 67.5% and 15.8 mg/g, respectively. The maximum removal efficiency and the adsorption capacity were obtained at pH 8. Beyond that, removal efficiency and the adsorption capacity decreased. The results may be explained by the attraction force principle between the negative surface of silica and the cationic dye (safranin) (Saleh et al. 2021c). At lower pH values, the production of hydrogen ions increases, thus the negative charge at the silica surface decrease, and the removal efficiency decreases. The concentration of hydroxyl groups in the solution increases as the pH rises. Thus the attractive force between the silica and the safranin increases and positively affects the removal efficiency. Beyond pH 8, the hydroxyl groups may be exchanged with the safranin ions thus safranin removal decreases. In previous work, the charge of nonliving lichen *Pseudevernia furfuracea* surface evolved positive at acidic conditions, and the removal efficiency of the cationic dyes was negatively affected (Koyuncu and Kul 2020). The removal of the cationic dye basic red 18 by the natural Turkish clay showed a similar trend (Fil et al. 2013). According to Bouras and colleagues (2021), the maximum

**Table 8** Isotherms parameters

| Isotherm | Parameter | Value |
|---|---|---|
| Langmuir | $K_L$ | 0.04464 ± 0.01122 |
| | $Q_{max}$ | 85.31597 ± 6.97941 |
| | $R^2$ | 0.96008 |
| Freundlich | $K_f$ | 14.518 ± 6.75463 |
| | $1/n$ | 0.31878 ± 0.10175 |
| | $R^2$ | 0.78204 |

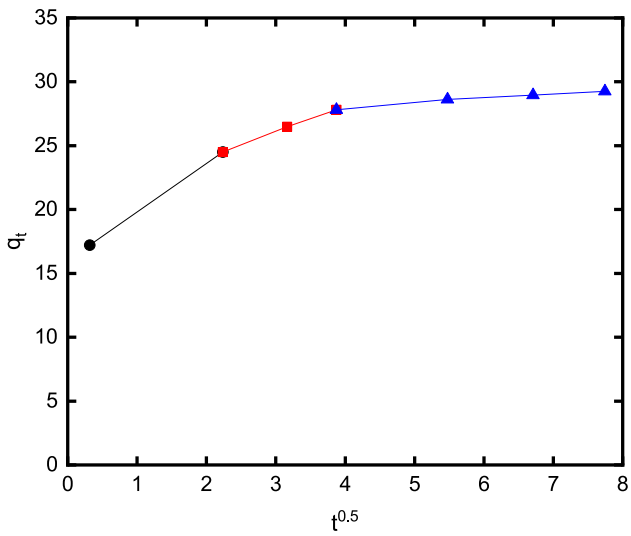


**Fig. 9** IDM for the adsorption of safranin dye onto the extracted silica

removal efficiency of methylene blue by *Aspergillus parasiticus* occurred at a pH value of 8 (Bouras et al. 2021).

### Adsorbent Amount Effects

The adsorbent amount effect on the removal efficiency was investigated. The extracted silica was added in different quantities (0.5–2.5 g/L) into solutions with a concentration of 25 mg/L and a pH value of 8. The mixtures were agitated (200 rpm) for 60 min at room temperature (25 ± 2 °C). The removal efficiency increased sharply with the increases in the adsorbent amount from 0.5 to 1.0 g/L from 50.64 to 78.00%. The result may be attributed to the increases in the adsorbent surface area or the availability of the active sites at the adsorbent surface. The further addition of the adsorbent amount did not significantly affect the removal efficiency. The adsorption capacity decreased with the increases in the adsorbent amount. Similar spectacles were obtained previously (Porkodi and Kumar 2007; Tahir and Rauf 2006). Figure 8 shows the changes in the removal efficiencies and the adsorption capacities with the adsorbent amount changes.

### Adsorption Isotherms

The nonlinear forms for the Langmuir and Freundlich were plotted with the aid of Origin software to have more precise results. The fitting results are shown in Table 8. The Langmuir correlation coefficient (0.96) is higher than the correlation coefficient for Freundlich isotherm (0.78). Thus the adsorption of safranin onto the extracted was described by Langmuir isotherm. According to Langmuir isotherm, the adsorption will occur in a monolayer in a homogenous manner. Langmuir also affirmed that the adsorbed molecules would be attached to the adsorbent surface in a finite number of the active sites, and not interacting between them will occur (Saleh et al. 2019b). Adebowale et al. (2014) utilized kaolinite clay to adsorb the safranin from the aqueous solution. In this context, Langmuir isotherm was used to describe the process (Adebowale et al. 2014). The removal of safranine dye from wastewater onto a waste-derived bio sorbent (seed of blackberry) was also best fitted to Langmuir isotherm (Ghosal and Singh 2020).

### Adsorption Mechanism

The adsorption mechanism was clarified via the intraparticle diffusion model (IDM). In this model, a graph was drawn between the adsorption capacities at different times versus the square root of the times, as shown in Eq. 8.

$$q_t = K_{\mathrm{IDM}} \times t^{1/2} + c \tag{8}$$

where $K_{\mathrm{IDM}}$ is the intraparticle diffusion model rate constant (mg/g min$^{1/2}$) and c is the boundary layer thickness.

The IDM graph for the adsorption of safranin dye onto the extracted silica is shown in Fig. 9. Accordingly, several notes can be noticed; the first is the multi-linearity with no interception through the origin point reflects that the film

**Table 9** Comparison with other adsorbents types

| Adsorbent | Adsorption capacity (mg/g) | References |
|---|---|---|
| Silica-based rice husk | 18.25 | This study |
| Kaolinite (nrk) clay | 16.23 | Adebowale et al. (2014) |
| Poly(vinylidene fluoride)-based nanofiber | 25.90 | Sharafinia et al. (2022) |
| Mesoporous adsorbent MCM-41 | 68.80 | Kaur et al. (2015) |
| Zinc oxide nanorod-loaded activated carbon | 32.06 | Sharifpour et al. (2018) |
| Pseudostem banana fibers | 21.87 | Sousa et al. (2014) |
| Rice husk (treated with NaOH) | 9.77 | Chowdhury et al. (2011) |
| Castor leaves-based biochar | 4.48 | Suleman et al. (2021) |

diffusion also had a role in the safranin adsorption, and the pore diffusion is not the only rate-controlling step. Also, the adsorption of safranin occurred in three stages. In the first step, the adsorption was fast due to the mass transfer of the safranin particles towards the adsorbent at the addition moment. The second stage is the film diffusion slowly from the boundary layer to the surface of the adsorbent. And finally, the movement of the adsorbate to the pores at the adsorbent surface.

### Comparison with Other Adsorbent Types

The removal of safranin from the aqueous solution via the adsorption techniques was reported previously. Li et al. (2021) adsorbed safranin onto polystyrene foam, which showed rapid adsorption, high adsorption capacity, and good reusability (Li et al. 2021). In another work, magnetic mesoporous clay was utilized for the same purpose. The adsorption capacity for the magnetic mesoporous clay was 18.48 mg/g (Fayazi et al. 2015). The nanomaterials were also used; the copper oxide nanoparticles (CuO-NP) obtained from pomegranate (*Punica granatum*) leaf extract achieved an adsorption capacity of 189.54 mg/g (Vidovix et al. 2021). Table 9 shows a brief comparison between the silica-based rice husk and other adsorbents types.

## Conclusion

In this study, the silica extraction from rice husk (RH) was optimized via the response surface methodology. The effects of temperature, potassium hydroxide to rice husk ratio (KOH: RH), and exposure time were modeled. The developed model was significant and adequately precise to navigate the design space with a percentage of 93.19%. Upon the model results, the KOH: RH ratio was the most important factor, followed by time, then temperature. The extracted silica was utilized for Safranin dye adsorption from aqueous solutions. The maximum safranin removal efficiency (78%) occurred at pH 8, adsorbent dose of 1 g/L, initial concentration of 25 mg/L, and contact time of 60 min. The Langmuir correlation coefficient (0.96) is higher than the correlation coefficient for Freundlich isotherm (0.78). Thus the adsorption of safranin onto the extracted was described by Langmuir isotherm.

The use of the extracted silica from rice husk as an adsorbent is a promising issue. Although the extracted silica was successfully utilized as an adsorbent, the extracted silica was used without any modifications. The presence of active hydroxyl groups in the extracted silica increases the functionality of the silica. In future research, the extracted silica can be modified in different ways. It may be attuned to high acidic systems or strongly alkaline systems. Also, it can be used as a template for high molecular weights polymers synthesis.

## References


Adebowale KO, Olu-Owolabi BI, Chigbundu EC (2014) Removal of Safranin-O from aqueous solution by adsorption onto kaolinite clay. J Encapsul Adsorp Sci 4:89–104

Alvarez J, Lopez G, Amutio M, Bilbao J, Olazar M (2014) Bio-oil production from rice husk fast pyrolysis in a conical spouted bed reactor. Fuel 128:162–169

Aly KI, Sayed MM, Mohamed MG, Kuo SW, Younis O (2020) A facile synthetic route and dual function of network luminescent porous polyester and copolyester containing porphyrin moiety for metal ions sensor and dyes adsorption. Microporous Mesoporous Mater 298:110063

Arslantaş C, Mbarek I, Saleh M, Isik Z, Ozdemir S, Dundar A, Dizge N (2022) Basic red 18 and remazol brilliant blue R biosorption using *Russula brevipes*, *Agaricus augustus*, *Fomes fomentarius*. Water Pract Technol, wpt2022008

Azimvand J, Didehban K, Mirshokraie S (2018) Safranin-O removal from aqueous solutions using lignin nanoparticle-g-polyacrylic acid adsorbent: synthesis, properties, and application. Adsorpt Sci Technol 36(7–8):1422–1440

Barker R, Dawe D, Tuong TP, Bhuiyan SI, Guerra LC (2000) The outlook for water resources in the year 2020: challenges for research on water management in rice production. Int Rice Comm Newsl 49:7–21

Bilici Z, Saleh M, Yabalak E, Khataee A, Dizge N (2022) The effect of different types of AOPs supported by hydrogen peroxide on the decolorization of methylene blue and viscose fibers dyeing wastewater. Water Sci Technol 85(1):77–89

Bouras HD, Rédayeddou A, Bouras N, Chergui A, Favier L, Amrane A, Dizge N (2021) Biosorption of cationic and anionic dyes using the biomass of *Aspergillus parasiticus* CBS 100926(T). Water Sci Technol 83(3):622–630

Box G, Hunter W, Hunter J (2005) Statistics for experimenters: an introduction to design, data analysis, and model building. Wiley, New York

Castillo X, Pizarro J, Ortiz C, Cid H, Flores M, De Cank E, Van Der Voort P (2018) A cheap mesoporous silica from fly ash as an outstanding adsorbent for sulfate in water. Microporous Mesoporpus Mater 272:184–192

Chen K, Wang JX, Dai YM, Wang PH, Liou CY, Nien CW, Wu JS, Chen CC (2013) Rice husk ash as a catalyst precursor for biodiesel production. J Taiwan Inst Chem Eng 44(4):622–629

Choudhary R, Venkatraman SK, Bulygina I, Senatov F, Kaloshkin S, Anisimova N, Kiselevskiy M, Knyazeva M, Kukui D, Walther F, Swamiappan S (2021) Biomineralization, dissolution and cellular studies of silicate bioceramics prepared from eggshell and rice husk. Mater Sci Eng C 118:111456

Chowdhury S, Misra R, Kushwaha P, Das P (2011) Optimum sorption isotherm by linear and nonlinear methods for safranin onto alkali-treated rice husk. Biorem J 15(2):77–89

de Sousa AÉA, Gomes ECC, de Quadros-Melo D, Diógenes ICN, Becker H, Longhinotti E (2014) Adsorption of safranin on pseudostem banana fibers. Sep Sci Technol 49(17):2681–2688

Deb A, Debnath A, Saha B (2019) Ultrasound-aided rapid and enhanced adsorption of anionic dyes from binary dye matrix

onto novel hematite/polyaniline nanocomposite: response surface methodology optimization. Appl Organometal Chem. 34:e5353
Della V, Hotza D, Junkes J et al (2006) Comparative study of silica obtained from acid leaching of rice husk and the silica obtained by thermal treatment of rice husk ash. Quim Nova 29:1175–1179
Fayazi M, Afzali D, Taher M, Mostafavi A, Gupta V (2015) Removal of Safranin dye from aqueous solution using magnetic mesoporous clay: optimization study. J Mol Liq 212:675–685
Feng Q, Chen K, Ma D, Lin H, Liu Z, Qin S, Luo Y (2018) Synthesis of high specific surface area silica aerogel from rice husk ash via ambient pressure drying. Colloids Surf A 539:399–406
Fil B, Karcioglu-Karakas Z, Boncukcuiglu R, Yilmaz A (2013) Removal of cationic dye (basic red 18) from aqueous solution using natural Turkish clay. Glob NEST J 15(4):529–541
Freundlich H (1906) Over the adsorption in solution. J Phys Chem 57:385–470
Ghosal D, Singh VK (2020) Study of the removal of Safranine-O dye from wastewater using waste derived biosorbent. Recent Innov Chem Eng 13(3):248–260
Gupta V, Suhas (2009) Application of low-cost adsorbents for dye removal: a review. J Environ Manag 90(8):2313–2342
Gupta V, Jain R, Mittal A, Mathur M, Sikarwar S (2007) Photochemical degradation of the hazardous dye Safranin-T using $TiO_2$ catalyst. J Colloid Interface Sci 309(2):464–469
Isik Z, Saleh M, Dizge N (2021) Adsorption studies of ammonia and phosphate ions onto calcium alginate beads. Surf Interfaces 26:101330
Jaya RP (2020) Porous concrete pavement containing nanosilica from black rice husk ash. New materials in civil engineering. Elsevier, pp 493–527
Kaur S, Rani S, Mahajan R, Asif M, Gupta VK (2015) Synthesis and adsorption properties of mesoporous material for the removal of dye safranin: Kinetics, equilibrium, and thermodynamics. J Ind Eng Chem 22:19–27
Khan MA (2015) Innovative ABC techniques. Accelerated bridge construction. Elsevier, pp 159–212
Korotkova TG, Ksandopulo SJ, Donenko AP, Bushumov SA, Danilchenko AS (2016) Physical properties and chemical composition of the rice husk and dust. Orient J Chem 32(6):3213–3219
Koyuncu H, Kul AR (2020) Removal of methylene blue dye from aqueous solution by nonliving lichen (*Pseudevernia furfuracea* (L.) Zopf.), as a novel biosorbent. Appl Water Sci 10:72
Langmuir I (1918) The adsorption of gases on plane surfaces of glass, mica and platinum. Am Chem Soc 40:1361–1403
Li W, Xie Z, Xue S, Ye H, Liu M, Shi W, Liu Y (2021) Studies on the adsorption of dyes, methylene blue, safranin T, and malachite green onto Polystyrene foam. Sep Purif Technol 276:119435
Lim JS, Manan ZA, Alwi SRW, Hashim H (2012) A review on utilisation of biomass from rice industry as a source of renewable energy. Renew Sustain Energy Rev 16(5):3084–3094
Marangon E, Kulzer FE, Cocco GD, Meichtry RS, Mendonça LC, Kosteski LE, Costa FBPD, Oliveira MDJDD (2021) Mortars produced with an environmentally sustainable rice HUSK silica: Rheological properties. J Clean Prod 287:125561
Mohamed MG, El-Mahdy AFM, Meng T-S, Samy MM, Kuo S-W (2020) Multifunctional hypercrosslinked porous organic polymers based on tetraphenylethene and triphenylamine derivatives for high-performance dye adsorption and supercapacitor. Polymers 12(10):2426
Moraes CA, Fernandes IJ, Calheiro D, Kieling AG, Brehm FA, Rigon MR, Filho JAB, Schneider IA, Osorio E (2014) Review of the rice production cycle: byproducts and the main applications focusing on rice husk combustion and ash recycling. Waste Manag Res 32(11):1034–1048
Morcali MH, Zeytuncu B, Yucel O (2013) Platinum uptake from chloride solutions using biosorbents. Mater Res 16(2):528–538
Muhammad A, İkbal M, Mahmood T (2013) A study on improving the performance of a research reactor's equilibrium core. Nucl Technol Radiat Protect 28(4):362–369
Nuamah A, Malmgren A, Riley G, Lester E (2012) Biomass co-firing. Reference module in earth systems and environmental sciences. Elsevier, pp 55–73
Pang D, Weng W, Zhou J, Gu D, Xiao W (2021) Controllable conversion of rice husks to Si/C and SiC/C composites in molten salts. J Energy Chem 55:102–107
Phonphuak N, Chindaprasirt P (2015) Types of waste, properties, and durability of pore-forming waste-based fired masonry bricks. Eco-efficient masonry bricks and blocks design, properties and durability. Elsevier, pp 103–127
Porkodi K, Kumar K (2007) Equilibrium, kinetics and mechanism modeling and simulation of basic and acid dyes sorption onto jute fiber carbon: eosin yellow, malachite green and crystal violet single component systems. J Hazard Mater 143:311–327
Pota G, Bifulco A, Parida D, Zhao S, Rentsch D, Amendola E, Califano V, Costantini A (2021) Tailoring the hydrophobicity of wrinkled silica nanoparticles and of the adsorption medium as a strategy for immobilizing lipase: an efficient catalyst for biofuel production. Microporous Mesoporous Mater 328:111504
Preethi S, Sivasamy A, Sivanesan S, Ramamurthi V, Swaminathan G (2006) Removal of safranin basic dye from aqueous solutions by adsorption onto corncob activated carbon. Ind Eng Chem Res 45(22):7627–7632
Quispe I, Navia R, Kahhat R (2017) Energy potential from rice husk through direct combustion and fast pyrolysis: a review. Waste Manag 59:200–210
Rodríguez-Restrepo Y, Ferreira-Santos P, Orrego C, Teixeira J, Rocha C (2020) Valorization of rice by-products: protein-phenolic based fractions with bioactive potential. J Cereal Sci 95:103039
Saleh M, Yalvaç M, Arslan H (2019a) Optimization of remazol brilliant blue R adsorption onto *Xanthium italicum* using the response surface method. Karbala Int J Modern Sci 5(1):8
Saleh M, Yalvaç M, Arslan H, Gün M (2019b) Malachite green dye removal from aqueous solutions using invader centaurea solstitialis plant and optimization by response surface method: kinetic, isotherm, and thermodynamic study. Eur J Sci Technol 17:755–768
Saleh M, Yildirim R, Isik Z, Karagunduz A, Keskinler B, Dizge N (2021a) Optimization of the electrochemical oxidation of textile wastewater by graphite electrodes by response surface methodology and artificial neural network. Water Sci Technol 84:1245–1256
Saleh M, Demir D, Ozay Y, Yalvac M, Bolgen N, Dizge N (2021b) Fabrication of basalt embedded composite fiber membrane using electrospinning method and response surface methodology. J Appl Polym Sci 138:50599
Saleh M, Isik Z, Yabalak E, Yalvac M, Dizge N (2021c) Green production of hydrochar nut group from waste materials in subcritical water medium and investigation of their adsorption performance for Crystal Violet. Water Environ Res 93:3075–3089
Saranya P, Sri-Gayathiri CM, Sellamuthu KM (2018) Potential use of rice husk ash for enhancing growth of maize (*Zea mays*). Int J Curr Microbiol Appl Sci 7(3):899–906
Shafie S, Mahlia T, Masjuki H, Ahmad-Yazid A (2012) A review on electricity generation based on biomass residue in Malaysia. Renew Sustain Energy Rev 16:5879–5889
Shah K (1998) Handbook of synthetic dyes and pigments. Multitech Publishing Co
Sharafinia S, Farrokhnia A, Lemraski EG (2022) Optimized safranin adsorption onto poly(vinylidene fluoride)-based nanofiber via response surface methodology. Mater Chem Phys 276:125407
Sharifpour E, Ghaedi M, Azad FN, Dashtian K, Hadadi H, Purkait M (2018) Zinc oxide nanorod-loaded activated carbon for

ultrasound-assisted adsorption of safranin O: central composite design and genetic algorithm optimization. Appl Organomet Chem 32(2):e4099

Suleman M, Zafar M, Ahmed A, Rashid M, Hussain S, Razzaq A, Mohidem N, Fazal T, Haider B, Park Y-K (2021) Castor leaves-based biochar for adsorption of safranin from textile wastewater. Sustainability 13:6926

Tahir S, Rauf N (2006) Removal of cationic dye from aqueous solutions by adsorption onto bentonite clay. Chemosphere 63:1842–1848

Thamnarathip P, Jangchud K, Nitisinprasert S, Vardhanabhuti B (2016) Identification of peptide molecular weight from rice bran protein hydrolysate with high antioxidant activity. J Cereal Sci 69:329–335

Van V, Rößler C, Bui D, Ludwig H (2014) Pozzolanic reactivity of mesoporous amorphous rice husk ash in portlandite solution. Constr Build Mater 59:111–119

Vasanth-Kumar K, Sivanesan S (2007) Sorption isotherm for safranin onto rice husk: comparison of linear and non-linear methods. Dyes Pigments 72:130–133

Vidovix TB, Quesada HB, Bergamasco R, Vieira MF, Vieira AMS (2021) Adsorption of Safranin-O dye by copper oxide nanoparticles synthesized from *Punica granatum* leaf extract. Environ Technol. https://doi.org/10.1080/09593330.2021.1914180

Wang M, Huang Y, Chiueh P, Kuan W, Lo S (2012) Microwave-induced torrefaction of rice husk and sugarcane residues. Energy 37:177–184

Wang X, Chen H, Fu X, Li S, Wei J (2017) A novel antioxidant and ACE inhibitory peptide from rice bran protein: Biochemical characterization and molecular docking study. LWT 75:93–99